Spectroscopic insight into carbon speciation and removal on a Cu/BEA catalyst during renewable high-octane hydrocarbon synthesis

Qiyuan Wu[#], Anh T. To[#], Connor P. Nash, Daniel P. Dupuis, Frederick G. Baddour, Susan E. Habas, Daniel A. Ruddy**

Catalytic Carbon Transformation & Scale-up Center, National Renewable Energy Laboratory, Golden, CO 80401.

[#]These authors contributed equally to the manuscript.

KEYWORDS. Dimethyl ether, high octane gasoline, coke formation, catalyst regeneration, *in situ* spectroscopy, Cu/BEA catalyst.

Conversion of methanol and dimethyl ether to high-octane gasoline catalyzed by beta zeolite (BEA) provides an opportunity for the production of high-quality fuels from renewable carbon sources (e.g., gasified biomass). Recent research demonstrated that a Cu-modified BEA zeolite catalyst (Cu/BEA) offered advantages over the unmodified BEA catalyst due to multifunctional Cu species that enabled incorporation of co-fed H_2, reactivation of light alkanes, and reduction of products from the aromatic hydrocarbon pool. The shift in hydrocarbon pool chemistry has the potential to influence the identity and relative composition of surface carbon species that are often

linked to deactivation. A detailed understanding of these carbon species is important to develop an effective and efficient regeneration procedure that can enable the transition from fundamental catalyst development to commercial application. Here, we applied complementary *ex situ* and *in situ* characterization techniques to compare the structures of surface carbon species on post-reaction Cu/BEA and unmodified BEA catalysts. Both catalysts contained acyclic and aromatic hydrocarbons along with graphitic carbon species. However, the post-reaction Cu/BEA catalyst had a lower polycyclic aromatic content, and further, the graphitic species were more hydrogenated and defective. It was also found that the presence of Cu promoted carbon removal at lower temperatures than for unmodified BEA through activation of O_2 by Cu oxide during thermal oxidation. The fundamental insight into the composition of surface carbon species enabled the design of an effective and efficient regeneration strategy for the DME homologation reaction over Cu/BEA, resulting in full recovery of the catalyst activity.

1. Introduction

The ongoing research into zeolite-catalyzed conversion of methanol (MeOH) and dimethyl ether (DME) to hydrocarbons offers an opportunity to utilize renewable carbon sources (e.g., methanol from gasified biomass) to produce value-added fuels and chemicals [1-4]. One recent development is the production of a high-value, high-octane gasoline (HOG) mixture consisting of branched hydrocarbons rich in 2,2,3-trimethylbutane (i.e., triptane) [5-8]. The DME homologation reaction to produce HOG employs a beta zeolite (BEA) catalyst at mild conditions of 175 – 225 °C and 1 – 10 atm in contrast to high temperatures and pressures (i.e., 300 – 500 °C and 20 atm) typically used in methanol-to-hydrocarbons (MTH) reactions.

Despite the lower severity operating conditions, the DME-to-HOG reaction over a BEA catalyst follows the typical chemistry in MTH reactions, involving three major stages: (i) initial C-C bond formation from DME/MeOH or trace amounts of hydrocarbon contaminants, (ii) auto-catalytic, dual-cycle olefin and aromatic hydrocarbon pool chemistry, and (iii) accumulation of polycyclic carbon species leading to deactivation. Direct C-C bond formation from surface methoxy species is considered to be important in the early stage of the reaction (i.e., induction period) to initiate the hydrocarbon pools [3, 9-12]. When sufficient hydrocarbon pool species have been formed, auto-catalytic olefin and aromatic hydrocarbon cycles become the dominant reaction pathways controlling the activity and product selectivity [3, 9, 13-15]. Zeolite topologies and reaction conditions are known to affect the structures of surface hydrocarbon species that contribute to both the olefin and aromatic cycles, resulting in changes to the observed product distribution. Under typical high-temperature conditions for MTH reactions (e.g., > 300 °C), the aromatic cycle is dominant in both small-pore zeolites such as SAPO-34 (composed of large 12-membered ring (12-MR) cavities interconnected by narrow 8-MR windows) and large-pore zeolites such as BEA (composed of 12-MR channels) [2, 3, 9, 15]. In contrast, the olefin cycle is dominant in the unidimensional 10-MR channels of ZSM-22, since the pores are not large enough for the aromatic pool to be active. The topological constraint of ZSM-22 results in a product mixture that is rich in C_{5+} hydrocarbons from carbon chain growth in the olefin cycle [2, 9, 15]. Both hydrocarbon pool cycles can operate simultaneously in HZSM-5 zeolite, which contains 10-MR pores for the olefin cycle and spacious intersections for the aromatic cycle, leading to a wide range of hydrocarbon products [2, 3, 9, 15]. On the other hand, Iglesia et al. have demonstrated that at low temperatures and high DME partial pressures, the olefin cycle is dominant for many solid acid catalysts, in which the relative stabilities of ion-pairs at transition states dictate the

selectivity to highly branched hydrocarbon products such as isobutane and triptane [5, 6, 8]. Under these conditions, hydride transfer with surface carbenium ions to form these alkanes also results in the formation of alkylated benzenes, especially hexamethylbenzene (HMB), decreasing the yield of desired products and deactivating the catalyst [5, 6, 16].

Aiming to improve HOG hydrocarbon yield from DME homologation, research from our laboratory demonstrated that addition of Cu to BEA zeolite (Cu/BEA) enabled incorporation of co-fed H_2 into the hydrocarbon products, resulting in a 2-fold increase in hydrocarbon productivity compared to unmodified BEA and reduced formation of alkylated benzenes from hydride transfer [13]. Metallic and ionic Cu species were critical to the improved performance, where metallic Cu facilitated hydrogenation of light olefins [13], preventing them from propagating the aromatic cycle via aromatization reactions, and the ionic Cu sites activated light paraffins for continued chain-growth in the olefin cycle [17, 18]. Further, we recently reported that the improved performance demonstrated by the Cu/BEA catalyst may lead to favorable process economics for the DME-to-HOG process over traditional, high-temperature methanol-to-gasoline processes [18].

Many research groups have sought to characterize the surface carbon species on zeolite catalysts after typical high-temperature (e.g. > 300 °C) MTH reactions, and the presence of a wide range of hydrocarbon species were identified by various spectroscopic methods such as UV-visible, infrared, Raman, and solid-state nuclear magnetic resonance (NMR) spectroscopies [2, 3, 9, 19-24]. As mentioned above, both zeolite topology and reaction conditions affect the structure of hydrocarbon pool species. For instance, under high-temperature MTH reaction conditions, heptamethylbenzenium and pentamethylcyclopentenyl cations were identified as the main catalytic engines for olefin formation from the aromatic cycle in BEA and SAPO-34 zeolites, respectively [23, 24]. In contrast, cyclopentenyl or cyclopentadienyl cations and

pentamethylbenzenium ions were identified as active species for olefin- and aromatic-based cycles in HZSM-5, respectively [25, 26] The active states of surface carbon species were also affected by reaction temperature. Methylated benzene species were found to be active in SAPO-34 at reaction temperatures up to 325 °C, while methylated naphthalene species were found to cause deactivation [27]. When the reaction temperature was increased to 500 °C, methylated naphthalenes were considered the active species, and deactivation was caused by polycyclic aromatics and extended carbon species [27].

The nature of the surface carbon species greatly impacts the catalyst stability and regenerability, which are critical to both fundamental and applied catalysis [28]. In the later stage of typical MTH reactions over zeolite catalysts, as mentioned above, carbon deposition is often identified as the major cause of the deactivation [9, 10, 14, 22]. Due to the hydrocarbon pool mechanism, active hydrocarbon species (e.g., monocyclic aromatics) can grow into inactive species (e.g., polycyclic aromatics and graphitic carbon) that cause deactivation by blocking accessibility to active sites [14, 22]. For the low-temperature DME-to-HOG reaction at 200 °C, we previously demonstrated the ability to operate for over 4-fold longer times-on-stream (TOS) for the Cu/BEA catalyst compared to unmodified BEA. With the BEA catalyst, the reactor plugged after 20 – 24 h due to the excessive formation of HMB, but with Cu/BEA no reactor plugging was observed after 100 h [18]. However, the identity of surface carbon species that may have resulted in improved lifetime of Cu/BEA was not investigated. Complementary to studies of catalyst deactivation, characterization of post-reaction catalysts and investigations into the removal of surface-bound species are often critical in the design of an effective and efficient regeneration procedure for the HOG process. Thus, fundamental differences in the speciation and composition

of surface carbon species for the low-temperature HOG synthesis reaction compared to typical high-temperature MTH reactions is of significant interest.

Herein, we report a detailed analysis of the speciation and oxidative removal of surface carbon on both post-reaction Cu/BEA and unmodified BEA catalysts. Utilizing complementary spectroscopic techniques, we identified reduced aromatic content, especially polycyclic aromatic hydrocarbons, in the post-reaction Cu/BEA catalyst compared to post-reaction BEA. Moreover, the graphitic carbon species in the post-reaction Cu/BEA catalyst were more hydrogenated and defective than those in the post-reaction BEA catalyst. The contribution of graphitic carbon is significantly reduced in the low-temperature DME-to-HOG reaction compared to high-temperature MTH reactions. Further, applying *in situ* characterization techniques, we determined that the addition of Cu significantly lowered the oxidation temperature for all carbon species. Based on these findings, a minimum oxidation temperature of 450 °C was identified, and an effective and efficient regeneration procedure for full recovery of DME homologation activity over the Cu/BEA catalyst was developed and demonstrated.

2. Experimental

2.1 General

Beta zeolite with a SiO_2/Al_2O_3 ratio of 27 (Si/Al = 13.5) and a particle size of 45 – 125 μm was obtained in ammonium form from Tosoh. It was calcined in flowing air at 550 °C to give the proton form (denoted as BEA). Supported Cu on BEA zeolite, denoted Cu/BEA, was prepared via an incipient wetness impregnation procedure as previously described [13], with 4.3 wt% Cu as determined by ICP-OES analysis. The catalyst was calcined *ex situ* in a box furnace in flowing air by heating at 2 °C/min to 500 °C and holding at this temperature for at least 6 h prior to use. DME

was purchased from Sigma-Aldrich. Compressed air, UHP H_2, UHP Ar, 5% H_2/95% N_2, 1% O_2/99% He and 95% H_2/5% Ar was purchased from Matheson gas. All gases were used without any further purification.

2.2 DME homologation reaction and post-reaction catalyst preparation

BEA and Cu/BEA powders were pressed, crushed in a porcelain mortar and pestle, and sieved to 212-300 μm pellets (50 – 70 mesh) for catalytic evaluation. The catalyst (0.6 g) was diluted with 3.6 g of low surface-area, inert silicon carbide (60 – 70 mesh) to achieve a constant catalyst bed volume and to minimize channeling, axial dispersion, and temperature gradients in the bed. Catalysts were loaded into a 7.9 mm ID stainless-steel tubular reactor and positioned within the isothermal zone using quartz chips and quartz wool. A four-point thermocouple positioned within the catalyst bed was used to monitor and control reaction temperature. The reaction temperature was maintained within ± 0.5 °C of the set point by a 3-zone furnace. The catalyst was reduced in flowing H_2 (25 sccm) by heating at 5 °C/min to 300 °C and holding at this temperature for at least 3 h before cooling to reaction temperature (200 °C). When the temperature was stabilized at 200 °C, the reactant mixture was introduced with flow rates of 6.1, 6.1, and 1.0 sccm for DME, H_2, and Ar, respectively, to achieve a weight hourly space velocity (WHSV) of 1.2 g_{DME}/g_{cat}/h, and H_2 to DME molar ratio of 1:1. Ar was used as an internal standard. Time on stream (TOS) is defined as the cumulative time elapsed from the start of DME flow. Reaction products were analyzed online by Agilent Technologies 7890B gas chromatographs equipped with flame ionization detectors and thermal conductivity detectors. The inlet gas composition was quantified at the conclusion of each experiment. Equations to calculate the conversion, yield, turnover number (TON), and selectivity are provided in the Supplementary Information. The catalysts were collected from the reactor after 20 h TOS for the BEA catalyst and 22 h TOS for

the Cu/BEA catalyst, separated from the silicon carbide, and denoted as post-reaction (PR) catalysts PR-BEA and PR-Cu/BEA, respectively.

2.3 Catalyst characterization

2.3.1 Thermogravimetric analysis coupled with Fourier transform infrared (TGA-FTIR) spectroscopy

TGA-FTIR spectroscopic analysis of PR catalysts was conducted using a SYS Evolution TGA instrument coupled with a Thermo Scientific Nicolet 6700 FTIR spectrophotometer. In a typical analysis, ca. 30 mg of PR catalyst was pretreated at 100 °C for 30 min in 50 sccm flowing N_2 to remove adsorbed moisture. Then, the carrier gas was switched to air (50 sccm) at 100 °C and held for 10 min to stabilize the baseline signals for both TGA and IR spectroscopy. The sample was then heated to 800 °C at 20 °C/min in flowing air. The derivative mass loss (dM/dT) data were obtained by differentiating the TGA data. IR spectra of the effluent gas were continuously collected (ca. 30 seconds per spectrum) in the range of 400 – 4000 cm^{-1} with a resolution of 4 cm^{-1}. The total intensity for each spectrum was determined from the integrated sum of all peaks and plotted versus time to generate a total product evolution profile. The profiles for CO_2, water, and hydrocarbons were determined by integrating a characteristic peak for each species: 2200 – 2400 cm^{-1} for CO_2, 1300 – 1900 cm^{-1} for water, and 2800 – 3100 cm^{-1} for hydrocarbons. Gaussian peaks and a constant baseline were used to fit the profiles. For the TGA-FTIR spectroscopic analysis of mixed PR-BEA and fresh Cu/BEA or mixed PR-BEA and PR-Cu/BEA catalysts, an equal mass of each catalyst was mixed and crushed together in a porcelain mortar and pestle to facilitate contact between the two materials. Then, the same analysis procedure was applied for ca. 40 mg of the catalyst mixture.

2.3.2 *In situ* diffuse reflectance ultraviolet-visible (DR-UV-vis) spectroscopy

In situ DR-UV-vis spectroscopy was conducted using an Agilent Cary 5000 UV-vis-NIR spectrophotometer equipped with a Harrick Praying Mantis *in situ* diffuse reflectance cell which allows a maximum temperature of ca. 475 °C when flowing room-temperature gases through the sample. DR-UV-vis spectra of the PR catalyst samples were collected over the range of 200 – 800 nm. The PR catalysts were first measured without any thermal treatment, then at varying temperatures up to 450 °C under 40 sccm air flow to study the evolution of surface hydrocarbon species during catalyst regeneration. The series of *in situ* spectra were normalized to the intensity at the cutoff wavelength of the windows on the *in situ* cell (250 nm). The DR-UV-vis spectra of the PR catalysts collected before *in situ* oxidation were fitted with multiple Lorentzian peaks in the range of 200 – 800 nm using a cubic baseline and the Multipeak Fitting package in the Igor Pro 8 software. To achieve the best fit, the number of peaks and peak positions were not constrained. The fitting results were then used to identify the position and area of all peaks. The relative percentages of the peak areas corresponding to different carbon species identified by DR-UV-vis spectroscopy in each PR catalyst were then calculated by dividing the area of the individual peak by the sum of the areas of all the peaks.

2.3.3 *In situ* Raman spectroscopy

In situ Raman spectroscopy was conducted using a Horiba Jobin Yvon Raman system equipped with a Linkam Scientific Instrument CCR1000 Catalyst Cell Reactor which allows a maximum temperature of ca. 475 °C when flowing room-temperature gases through the sample. A 325 nm UV laser was used as the excitation source. Raman spectra were collected under 40 sccm flowing Ar after exposure to 10 sccm flowing air for 30 minutes at varying temperatures up to 450 °C to prevent laser-promoted oxidation during analysis. Each spectrum was normalized to the intensity of the elastic scattering band (0 cm^{-1}) in each spectrum. The region of interest (1000

– 2400 cm^{-1}) in the Raman spectra of the PR catalysts collected before *in situ* oxidation were fitted with two Lorentzian peaks using a constant baseline and the Multipeak Fitting package in the Igor Pro 8 software. The position of each Raman band was then directly obtained from the fitting results and the ratio between two Raman bands was calculated using the fitted peak areas.

2.3.4 X-ray diffraction (XRD)

Powder XRD patterns were collected using a Rigaku Ultima IV diffractometer with a Cu Kα source (40 kV, 44 mA). Powder samples were supported on a glass sample holder with a 0.5 mm recessed sample area and were pressed into the recession with a glass slide to obtain a uniform z-axis height. XRD patterns were collected in the 2θ range of 10 to 60° at a scan rate of 2°/min. Diffraction patterns were compared to powder diffraction files from the International Centre for Diffraction Data (ICDD).

2.3.5 ^{27}Al nuclear magnetic resonance (NMR) spectroscopy

Magic angle spinning (MAS) ^{27}Al NMR single pulse spectra were acquired using a Bruker Advance III 600 MHz (14.1 T) spectrometer using 2.5 mm outer diameter zirconia rotors and a MAS rotation frequency of 15 kHz. Spectra were accumulated from 8,192 scans and externally referenced to a sample of Al_2O_3 with a chemical shift of 16.0 ppm. The analyzed samples were not dehydrated prior to analysis.

2.3.6 Transmission electron microscopy (TEM)

TEM imaging was performed using a FEI Tecnai G2 ST30 TEM operated at 300 kV. The catalyst was reduced in flowing 5% H_2/N_2 (500 sccm) by heating at 5 °C/min to 300 °C and holding for 1 h. After cooling to room temperature in flowing H_2, the catalyst was passivated in flowing 1% O_2/He (500 sccm) for 2 h before rapidly transferring to an N_2 filled glovebox. The reduced and

passivated catalyst was dispersed in dry hexanes under air-free conditions and drop-cast onto a lacey carbon-coated Cu mesh grid (Ted Pella part no. 01895-F). Air exposure was minimized prior to TEM imaging.

2.4 Catalyst regeneration evaluation

Catalyst regeneration was performed after 24 h of DME homologation reaction with sequential oxidative and reductive treatments. The DME homologation reaction was performed as described above, and then the reactor was cooled from reaction temperature of 200 °C to 150 °C in flowing Ar (5 sccm). Once the reactor temperature was stabilized at 150 °C, Ar flow was stopped and air was introduced at 25 sccm. The temperature was increased from 150 °C to 450 °C at 2 °C/min, and held at 450 °C for 8 h, before cooling to 300 °C. Once the reaction temperature was stabilized at 300 °C, air flow was stopped, and the reactor was flushed with 5 sccm of Ar for 30 min. The catalyst was then reduced in flowing 95% H_2/5% Ar (25 sccm) at 300 °C for 3 h before cooling to 200 °C for the second DME homologation reaction cycle. After 24 h of reaction in the second cycle, the catalyst was regenerated again following the same procedure as above, with oxidative treatment in air at 500 °C and reductive treatment in 95% H_2/5% Ar at 300 °C, before the third DME homologation reaction cycle.

3. Results and Discussion

3.1 Identification of carbon species on post-reaction (PR) catalysts

To generate PR catalyst samples for characterization of surface carbon species, DME homologation was performed at 200 °C and atmospheric pressure over the Cu/BEA and BEA zeolite catalysts for 22 and 20 h, respectively, at which times the activity of the catalysts reached steady state. Consistent with prior reports [13, 17, 18], the Cu/BEA catalyst exhibited notably

higher activity than the BEA catalyst, highlighted by maximum DME conversion (16.3% vs 6.5%; Fig. S1A), gravimetric activity (Fig. S1C, 0.12 vs 0.05 $g_{HC}/g_{cat}/h$) and cumulative turnover number (TON) at ca. 20 h TOS (Fig. S1B, 90 vs 13 mol_C/mol_{H+}). The product carbon selectivities over the Cu/BEA and BEA catalysts were similar, as expected (Fig. S1D). The PR-Cu/BEA and PR-BEA catalysts were collected for investigation into the structure and composition of surface carbon species and to understand carbon removal during catalyst regeneration.

DR-UV-vis spectroscopy was employed to initially identify the molecular hydrocarbon species on the PR catalysts. Three peaks, centered at 300, 380, and 456 nm were present in the DR-UV-vis spectra of both PR-Cu/BEA and PR-BEA samples (Fig. 1A). These peaks are similar to those corresponding to surface hydrocarbons on zeolite catalysts identified after short TOS for high-temperature MTH reactions, and representative structures are included Table 1 [3, 19, 22, 29, 30]. The peak at 300 nm is attributed to monoenylic and cyclopentenyl carbenium ions, the broad peak at 380 nm to a combination of dienylic (367 nm) and methylated benzene carbenium (385 nm) ions, and the peak at 456 nm to trienylic carbenium ions. An important difference was observed in the spectrum of PR-BEA, which included a shoulder peak at 420 nm corresponding to polycyclic aromatic species, including methylated naphthalene carbenium ions [27]. These polycyclic aromatic species were not observed in the spectrum of PR-Cu/BEA. In a typical high-temperature MTH reaction, the peaks at 300, 380, and 456 nm were observed at early TOS and started to broaden after 1 – 3 h of reaction [14, 22]. The peak broadening then extended to absorbance over a wider range of wavelengths and the catalysts visibly darkened in color due to the deposition of large/extended carbon species on the outer surface of the zeolite [14, 22]. This type of extended carbon hinders detailed analysis of DR-UV-vis spectra and suggests that graphitic carbon (i.e., coke) is the dominant species after high-temperature MTH reactions [31, 32]. In

contrast, at the lower reaction temperature of 200 °C studied here, peak broadening was minimal for both PR-Cu/BEA or PR-BEA catalysts after 20 h TOS, suggesting limited graphitic carbon content on the external zeolite surface, thus allowing for analysis of the relative composition of the molecular species. The DR-UV-vis spectra for PR-Cu/BEA and PR-BEA catalysts were fitted with multiple peaks based on the species identified above, and the relative composition of each species was then calculated (Figs. 1B, S2A, S2B, and Table 1) [14]. For the PR-Cu/BEA catalyst, the monoenylic species were most abundant (39%). Di- and tri-enylic species accounted for 30% of the total peak area, and the monocyclic aromatic species contributed 31%. Importantly, there was no contribution from polycyclic aromatics (Fig. 1B and Table 1). In contrast, for the PR-BEA catalyst, monoenylic species constituted only 16%, while monocyclic aromatic species contributed 7% and polycyclic aromatic species had the greatest contribution at 49%. The lower total aromatic content, especially polycyclic aromatic content, deposited on the PR-Cu/BEA catalyst compared to PR-BEA is consistent with previously reported observations over the Cu/BEA catalyst: (i) reduced HMB formation [13], (ii) promotion of the olefin cycle over the aromatic cycle [13], and (iii) operation for longer TOS without reactor plugging [18].

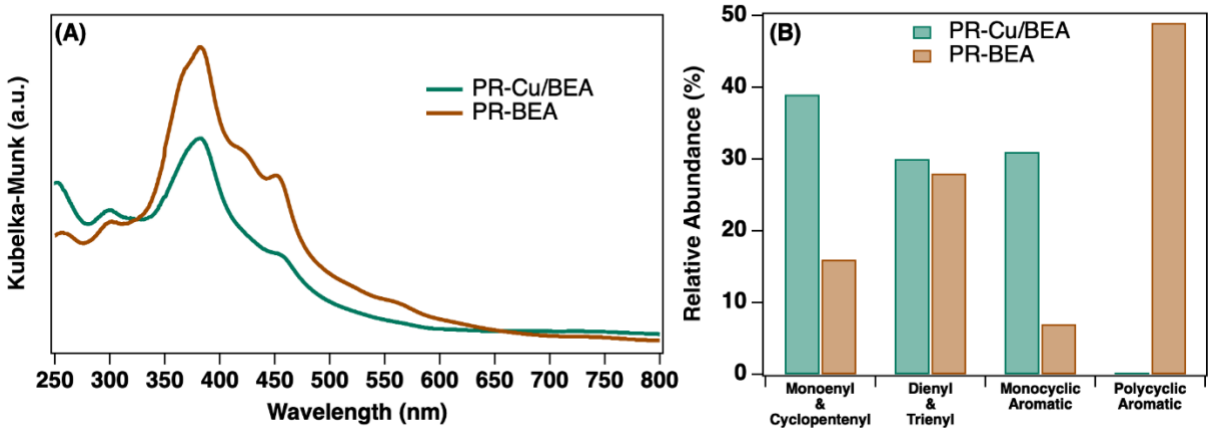

Fig. 1. (A) DR-UV-vis spectra of PR-Cu/BEA and PR-BEA catalysts. (B) Relative surface

hydrocarbon composition of PR-Cu/BEA and PR-BEA catalysts obtained from fitting of DR-UV-vis spectra.

Table 1 DR-UV-vis peak assignments and positions for PR catalysts.

Hydrocarbon species	Representative structure	Peak position	Composition	
			PR-Cu/BEA	PR-BEA
Monoenyl	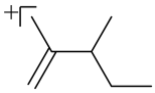	300 nm	39%	16%
Cyclopentenyl	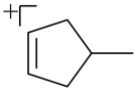			
Dienyl	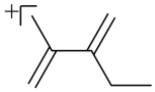	367 nm	30%	28%
Trienyl	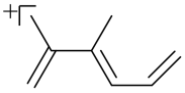	456 nm		
Monocyclic Aromatic	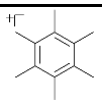	385 nm	31%	7%
Polycyclic Aromatic	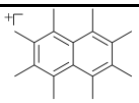	420 nm	0%	49%

The absence of a broad absorbance across the visible region of the DR-UV-vis spectra for both the PR-Cu/BEA and PR-BEA catalysts suggests that the relative quantity of graphitic carbon species deposited on the catalysts during the low-temperature DME-to-HOG reaction is less than that for typical high-temperature MTH reactions. However, during the peak fitting of the DR-UV-vis spectra, it was found that a non-linear baseline with a broad peak shape (Figs. S2A and S2B) was necessary to obtain appropriate fits. Such a baseline suggests that extended carbon species are likely present in the PR-Cu/BEA and PR-BEA catalysts, but at quantities too small to be directly

observed in the DR-UV-vis spectra given that the extinction coefficient of graphitic carbon [33] is significantly lower than those of hydrocarbon molecules [34]. Complementary to DR-UV-vis spectroscopy for the identification of molecular hydrocarbon species, Raman spectroscopy was utilized to characterize extended carbon species (i.e., graphitic carbon) [35]. In the Raman spectra of both the PR-Cu/BEA and PR-BEA catalysts (Fig. 2), features that correspond to the D band (centered at ca. 1380 cm^{-1}) and G band (centered at ca. 1585 cm^{-1}) of defective (i.e., partially hydrogenated) graphitic carbon species were observed [35]. The position of the G band in the spectrum for PR-Cu/BEA (1580 cm^{-1}) was at a lower wavenumber than that for PR-BEA (1588 cm^{-1}), indicating that the graphitic carbon species on the PR-Cu/BEA catalyst were more hydrogenated. This conclusion is also supported by the greater D:G ratio for the PR-Cu/BEA catalyst (1.3 for PR-Cu/BEA vs 1.1 for PR-BEA) [36]. Additionally, a shoulder (S) band in the range of 1180 – 1200 cm^{-1} corresponding to molecular aromatic species with large carbon rings was observed for both PR catalysts [37]. Fitting details for PR-Cu/BEA and PR-BEA are provided in Figs S2C, S2D, and Table S1. The Raman spectroscopy analysis of the PR catalysts indicates that extended carbon species still form during the low-temperature DME-to-HOG reaction, similar to high-temperature MTH reactions [14, 27, 38], albeit at much lower abundance, as determined by DR-UV-vis spectroscopy.

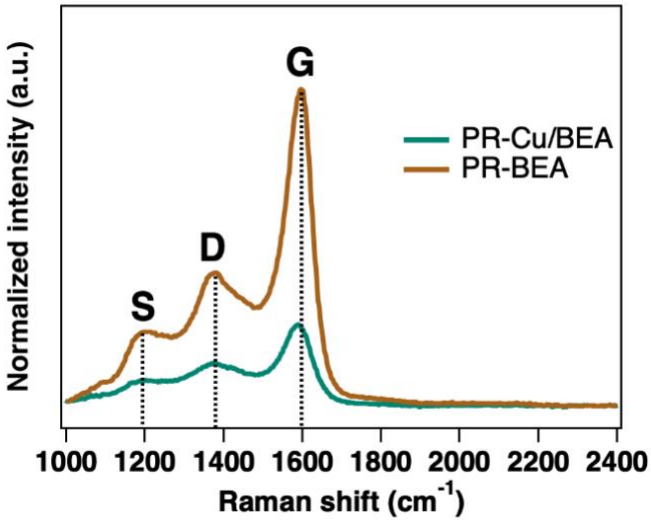

Fig. 2. Raman spectra of PR-Cu/BEA and PR-BEA catalysts with S band, D band, and G band assignments.

The combined results from DR-UV-vis and Raman spectroscopies of the PR catalysts after the low-temperature DME-to-HOG reaction indicated the presence of a range of surface carbon species that were predominantly acyclic hydrocarbons and aromatic hydrocarbons, with a contribution from defective, partially hydrogenated graphitic species. This complex composition of surface carbon species is comparable to that commonly observed on catalysts after high-temperature MTH reactions; however, the DR-UV-vis spectra suggest a markedly lower contribution from graphitic carbon species after the low-temperature DME-to-HOG reaction studied here. Comparing the PR-BEA and PR-Cu/BEA catalysts, the presence of polycyclic aromatics on PR-BEA and absence of these species on PR-Cu/BEA is a key difference that is anticipated to impact removal of the carbon species from the PR catalysts.

3.2 Oxidation of carbon species

To inform the conditions required for carbon removal towards catalyst regeneration, a coupled TGA-FTIR spectroscopic analysis of the PR catalysts in flowing air was performed and the results are shown in Figs. 3 and S3 – S6. For the PR-Cu/BEA catalyst, mass loss accounting for 9.5 wt% of the catalyst mass occurred between 200 and 500 °C, and the gaseous products identified in the FTIR spectra were CO_2 and water from oxidation of surface carbon species (Figs. 3A, S3B and S5A). In contrast, mass loss from the PR-BEA catalyst occurred in two stages (Figs. 3B and S4) with different gaseous product compositions. Between 200 and 360 °C, a mass loss of 3.5 wt% was observed. In addition to CO_2 and water, the FTIR spectra of the gaseous products from this initial mass loss indicated the presence of unoxidized hydrocarbons, evidenced by an absorption band at 2800 – 3200 cm^{-1} that was comparable to the infrared spectrum of branched C_7 hydrocarbons, one of the major hydrocarbon products from the DME-to-HOG reaction (Figs. 3B, S3D, S5B and S6). The second stage of mass loss occurred between 400 – 700 °C, and an additional 5.5 wt% was lost. The gaseous products identified in the FTIR spectra were the expected CO_2 and water from complete oxidation of surface carbon species (Figs. 3B, S3D and S5C). The TGA-FTIR profile of the PR-BEA catalyst (Fig. 3B) was comparable to temperature-programmed oxidation of catalysts after high-temperature MTH reactions, where the maximum of carbon removal occurred at 580 – 650 °C [39-41]. This high-temperature oxidation event is usually attributed to the oxidation of "hard coke" or polycyclic aromatic hydrocarbons [40]. In contrast, the TGA-FTIR profile of PR-Cu/BEA was unique in that the maximum of CO_2 evolution was observed at a much lower temperature of 400 °C (Figs. 3A and S4). The removal of the complex surface carbon species identified using DR-UV-vis and Raman spectroscopies was further explored using *in situ* spectroscopy (*vide infra*).

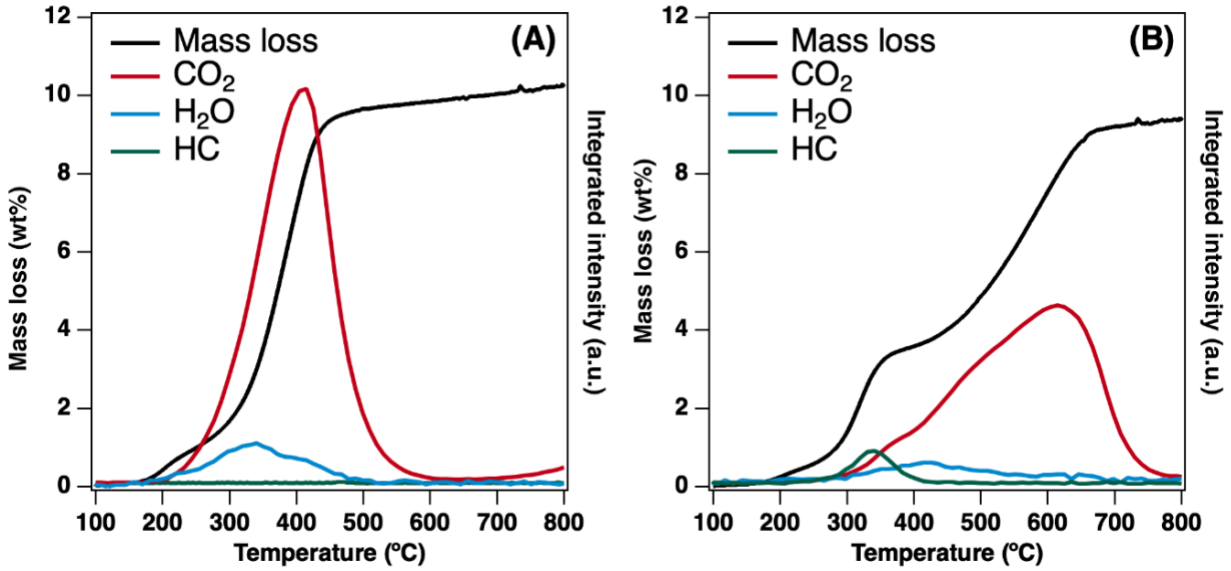

Fig. 3. TGA-FTIR spectroscopic analysis of oxidation of surface carbon species for (A) PR-Cu/BEA and (B) PR-BEA catalysts with temperature-resolved mass loss and integrated FTIR band intensity of gaseous products, CO_2, H_2O and hydrocarbons (HC). Data shown here were collected in flowing air.

TGA-FTIR spectroscopic analysis demonstrated that the required temperature for oxidation of carbon species on the PR-Cu/BEA catalyst (peak mass loss at 400 °C) was significantly lower than that for the PR-BEA catalyst (peak at 600 °C). Given the lower aromatic content and more-hydrogenated graphitic carbon on PR-Cu/BEA identified using DR-UV-vis and Raman spectroscopy, the lower oxidation temperature is not unexpected [42]. However, the 200 °C difference in carbon oxidation temperature was substantial and led to the hypothesis that Cu species may activate oxygen at lower temperature to aid carbon oxidation. To investigate this concept, two analogous oxidative TGA-FTIR experiments were conducted using physical mixtures of PR-BEA and fresh (oxidized without reduction) Cu/BEA catalysts or PR-BEA and PR-Cu/BEA (after exposure to air) catalysts with mass ratios of 1:1. Despite the reduced physical

proximity between the carbonaceous species on PR-BEA and Cu oxide on fresh Cu/BEA or PR-Cu/BEA, the presence of Cu oxide enabled carbon oxidation at lower temperature (Fig. 4). The maximum of CO_2 and water evolution occurred at ca. 400 °C, similar to that observed for PR-Cu/BEA (Figs. 3A and 4). It is worth noting that the low-temperature CO_2 evolution (ca. 400 °C) was relatively greater for the mixture of PR-BEA and PR-Cu/BEA (Fig. 4B) compared to PR-BEA and fresh Cu/BEA (Fig. 4A) due to the oxidation of carbon species from PR-Cu/BEA.

The TGA-FTIR profiles in Fig. 4 indicated that the presence of Cu oxide on either fresh Cu/BEA or PR-Cu/BEA promoted the oxidation of carbon species from PR-BEA at lower temperature compared to the carbon removal profile from PR-BEA without Cu. Supported Cu oxide has been reported to catalyze oxidation of volatile organic compounds, and we propose that similar reactions are occurring during the carbon removal explored here [43-45]. TGA-FTIR analysis of the PR catalysts conducted under inert gas flow demonstrated that similar unoxidized (i.e., branched C_7) hydrocarbons were observed in the FTIR spectra for both the PR-Cu/BEA and PR-BEA catalysts (Fig. S7). These "lighter" molecular hydrocarbon species, consistent with those identified by DR-UV-vis spectroscopy on both PR-Cu/BEA and PR-BEA, were oxidized when volatilized in the presence of Cu oxide and oxygen, as observed in Figs. 3A and 4. The graphitic carbon identified on both PR catalysts by Raman spectroscopy could be directly oxidized if in close proximity to Cu oxide, and this may be a pathway for carbon removal from PR-Cu/BEA. Alternatively, for both PR catalysts, cracking of these "heavier" species, including polyaromatics identified on PR-BEA by DR-UV-vis spectroscopy, to light hydrocarbon fragments and subsequent oxidation by Cu oxide represents a pathway that would lead to the lower temperature carbon removal that was observed. It is important to note that a portion of the carbon species in PR-BEA still required higher temperature (ca. 600 °C) for removal, which may be due to

insufficient proximity between Cu oxide and carbon species and/or the inherent higher temperatures needed for oxidation of the polycyclic aromatics and graphitic carbon species on the PR-BEA catalyst identified by DR-UV-vis and Raman spectroscopies.

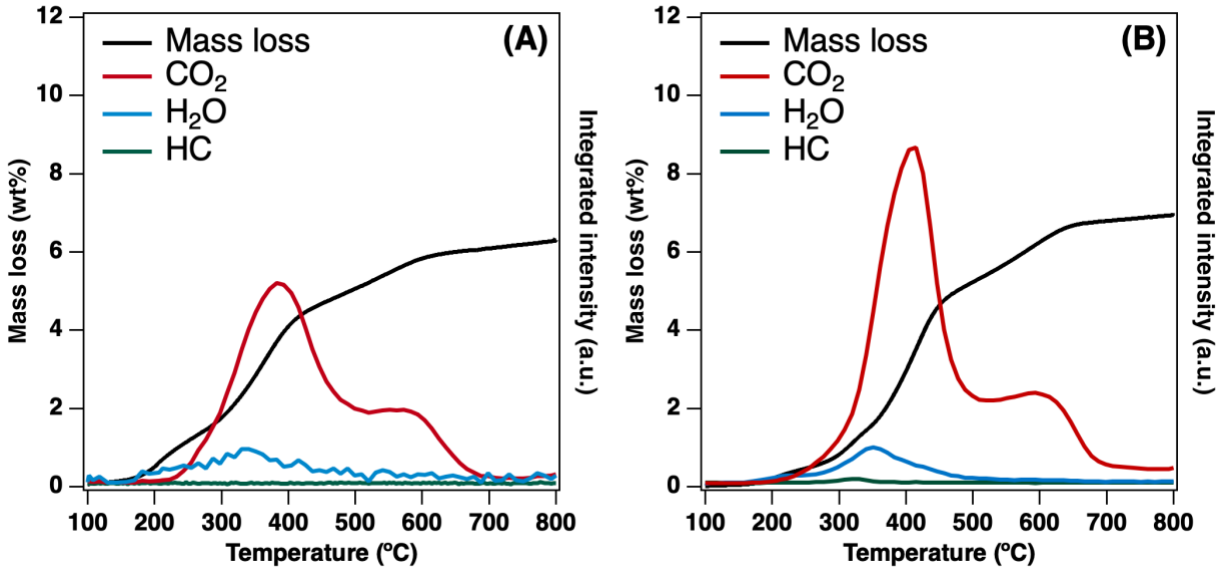

Fig. 4. TGA-FTIR spectroscopic analysis of oxidation of surface carbon species on a physical mixture of (A) PR-BEA + fresh Cu/BEA catalysts (50:50 mass ratio) and (B) PR-BEA + PR-Cu/BEA catalysts (50:50 mass ratio) with temperature-resolved mass loss and integrated FTIR band intensity of gaseous products, CO_2, H_2O and hydrocarbons (HC). Data shown here were collected in flowing air.

The observation of carbon removal at different temperatures for PR-BEA and PR-Cu/BEA motivated the application of *in situ* spectroscopies to follow the evolution/removal of each type of surface carbon species. The PR catalysts were heated in flowing air from room temperature to 450 °C, which was sufficient to remove surface carbon species from PR-Cu/BEA and is near the operational limit for the *in situ* cells. The *in situ* DR-UV-vis spectra for the PR-Cu/BEA catalyst (Fig. 5A) indicated that heating for 30 min at 250 °C resulted in greatly decreased intensity for all

three peaks at 300, 380, and 456 nm corresponding to monoenylic, dienylic and methylated benzene, and trienylic species, respectively. The removal of hydrocarbon species at this temperature is in agreement with the TGA-FTIR results, where substantial oxidation products were observed at temperatures near 250 °C. The spectrum after oxidation at 450 °C for 30 min was free from peaks related to hydrocarbon species and the only features present were the absorption edge at ca. 300 nm and the broad band at 700 – 800 nm, which are characteristic absorbance features of CuO and isolated Cu^{2+} species, respectively, in the Cu/BEA catalyst [46, 47]. On the other hand, in the case of PR-BEA catalyst, the intensity of peaks corresponding to surface hydrocarbon species did not decrease until the catalyst was oxidized at 350 °C for 30 min (Fig. 5B). Moreover, the removal of polycyclic aromatic species required temperatures up to 450 °C. Consistent with the TGA-FTIR spectroscopic analysis, the broad residual absorbance following oxidation at 450 °C for 30 min indicated that 450 °C was not sufficient to completely remove the surface carbon species on PR-BEA catalyst. As mentioned above, a broad absorbance in the DR-UV-vis spectra was assigned to extended carbon species in the case of high-temperature MTH reactions [14]. This type of broad absorbance was only observed in the *in situ* spectra of PR-BEA after removal of the molecular hydrocarbon species at 450 °C, strengthening the assignment of molecular species as the dominant carbon species in the DR-UV-vis spectra (Fig. 5B). Additionally, as mentioned previously, the extinction coefficient of graphitic carbon [33] is significantly lower than those of hydrocarbon molecules [34]. Thus, in the case of high-temperature MTH reactions where the broad absorbance is the dominant feature in UV-vis spectra, the quantity of extended carbon species must be significantly larger than that of molecular hydrocarbon species. Whereas, in the case of the low-temperature DME-to-HOG reaction, the well-defined peaks corresponding to molecular

hydrocarbon species suggests that the relative amount of deposited graphitic carbon species is much lower than that from high-temperature MTH reactions.

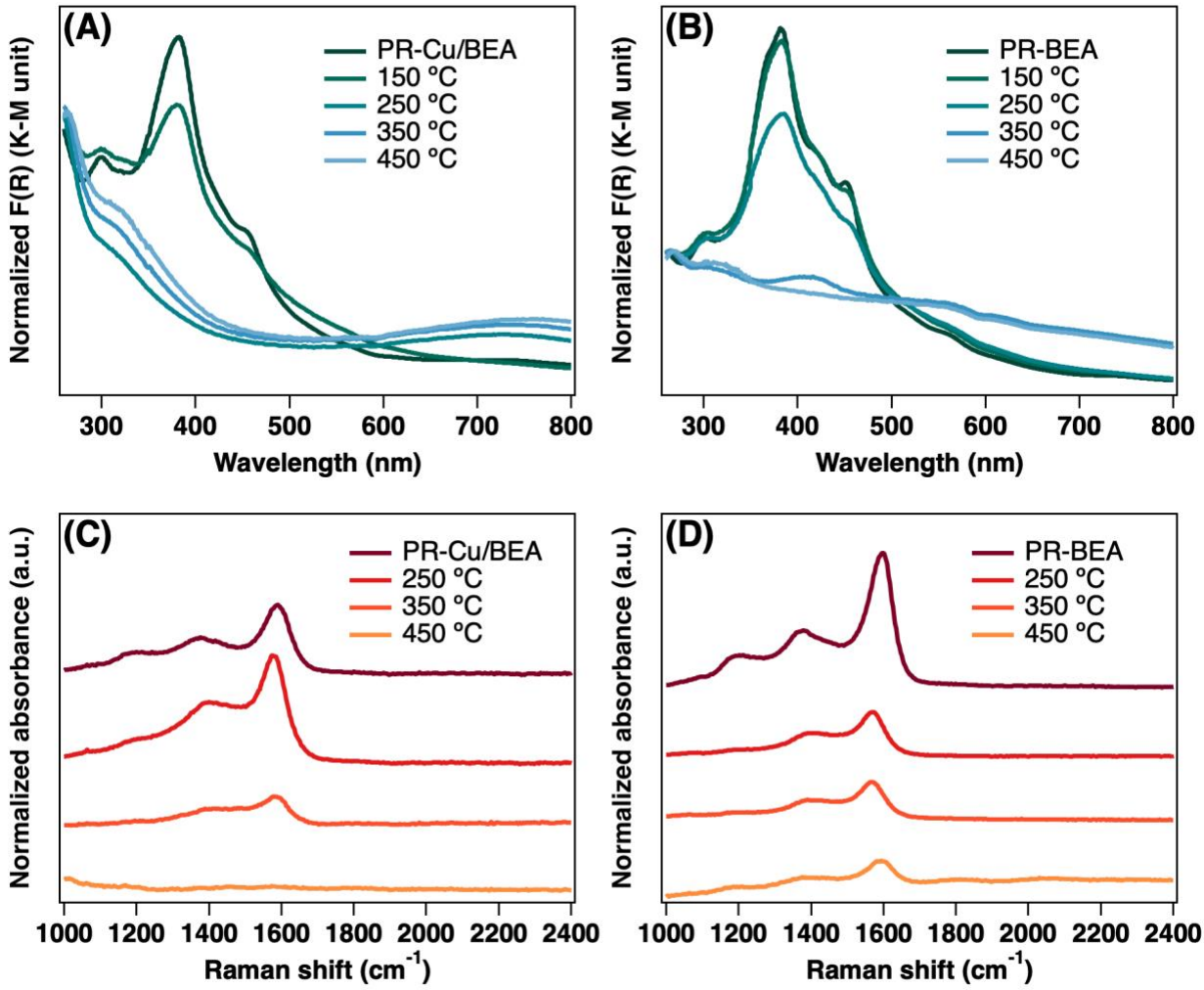

Fig. 5. *In situ* spectroscopic investigation of residual carbon species on PR-Cu/BEA and PR-BEA catalysts following oxidation in air at increasing temperatures for 30 min. *In situ* DR-UV-vis spectra of (A) PR-Cu/BEA and (B) PR-BEA catalysts, and *in situ* Raman spectra of (C) PR-Cu/BEA and (D) PR-BEA catalysts.

The oxidation of graphitic carbon species on PR catalysts was monitored using *in situ* Raman spectroscopy. For both PR-Cu/BEA and PR-BEA, species corresponding to the S bands were removed at lower temperature (350 °C) than those corresponding to the D and G bands. For PR-Cu/BEA, intensities of bands for graphitic carbon species began to decrease at 350 °C and were fully removed after heating at 450 °C (Fig. 5C). These *in situ* Raman spectra highlight the higher temperature needed to fully remove graphitic carbon in comparison to molecular hydrocarbon species, which were fully removed at 250 °C, as demonstrated above using *in situ* DR-UV-vis spectroscopy (Fig. 5A). The difference in required temperature to remove molecular hydrocarbon and graphitic carbon in PR-Cu/BEA agreed well with the continuous mass loss and CO_2 evolution observed by TGA-FTIR spectroscopy. In the case of the PR-BEA catalyst, the graphitic carbon was not completely removed after treatment at 450 °C (Fig. 5D), consistent with the TGA-FTIR spectroscopic data showing mass loss and CO_2 evolution through 700 °C.

The combination of TGA-FTIR spectroscopy and *in situ* DR-UV-vis and Raman spectroscopies demonstrated that the addition of Cu to BEA zeolite not only reduced the total aromatic content, especially polycyclic aromatic hydrocarbons, but also promoted the oxidation of all surface carbon species by activating oxygen. Therefore, complete removal of carbon species was achieved at 200 °C lower for PR-Cu/BEA (450 °C) than for PR-BEA (> 650 °C). Higher temperatures were required to remove both the molecular hydrocarbon species and the graphitic carbon species from PR-BEA. A temperature greater than 550 °C is typically required for non-catalytic carbon removal during regeneration of catalysts [48] including zeolite catalysts after high-temperature MTH reactions (600 – 700 °C) [2, 49]. Thus, the addition of Cu both enhanced the catalytic performance for the DME-to-HOG reaction and enabled removal of residual carbon at a lower temperature, which is beneficial for catalyst lifetime and process economics [18].

3.3 Catalyst performance with forced regenerations

Insights into the speciation and structure of carbon deposits and the removal of these species during oxidation provided by *ex situ* and *in situ* characterization techniques enabled the design of a carbon removal procedure for the Cu/BEA catalyst. In order to investigate the recovery of catalytic performance after carbon removal, a series of forced regenerations were performed. The catalyst was subjected to the regeneration procedure after 24 h TOS, which is the same reaction period used to prepare the PR catalysts, and therefore, the catalyst is assumed to contain the carbon species described above. This reaction time allowed the catalyst to reach steady state activity but did not lead to complete deactivation. Following the typical hydrocarbon pool chemistry over Cu/BEA, the DME conversion and hydrocarbon product yield increased with TOS over the initial 3-5 h, attributed to the accumulation of the hydrocarbon pool species during induction period (Figs. 6A and S1A). After reaching a maximum in activity, deactivation occurred over the next 4 – 6 h (i.e., 4 – 10 h TOS), attributed to carbon species affecting the strong and highly dense acid sites [20]. The catalyst activity was relatively stable after 10 h TOS, evidenced by little change in activity or product selectivity (Figs. 6B and S8A).

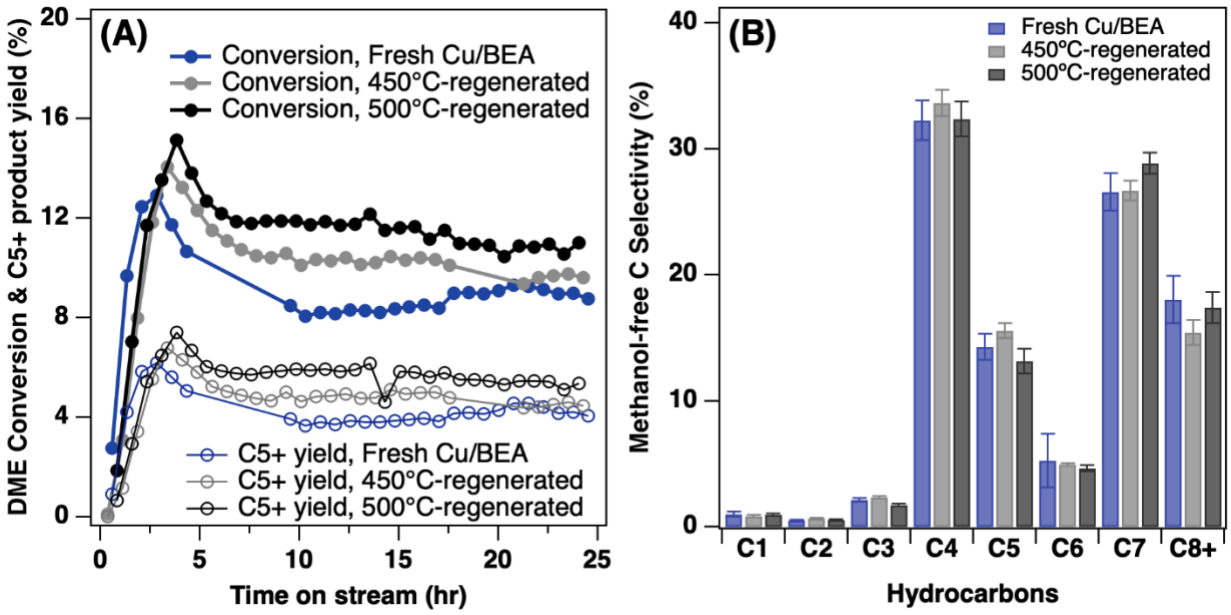

Fig. 6. (A) DME Conversion and C_{5+} hydrocarbon yield as a function of time during the DME-to-HOG reaction with co-fed H_2 over Cu/BEA before and after forced regeneration procedures. (B) Carbon selectivity grouped by carbon number before and after regeneration procedures. Product selectivity reported as the average of data points at 21 – 24 h TOS, with error bars representing 99% confidence intervals. Reaction conditions: 200 °C, 0.8 atm, WHSV of 1.2 $g_{DME}/g_{cat}/h$, and H_2:DME molar ratio of 1:1.

The first forced regeneration procedure consisted of an oxidation at 450 °C for carbon removal, as informed by characterization results above, followed by reduction at 300 °C to activate Cu prior to resuming the DME-to-HOG reaction. To compare the effect of oxidation temperature on regeneration, an additional forced regeneration cycle was performed with an oxidation at 500 °C. Analysis by XRD and ^{27}Al NMR spectroscopy of PR-Cu/BEA sample with and without regeneration at 500 °C (Figs. 7A and 7B) confirmed that the zeolite framework retained its crystallinity and no dealumination was observed after carbon removal. In addition, TEM imaging

showed a distribution of Cu particle sizes after the oxidation-reduction cycles (Figs. 7C and 7D) that was consistent with TEM analysis of the fresh reduced catalyst [13].

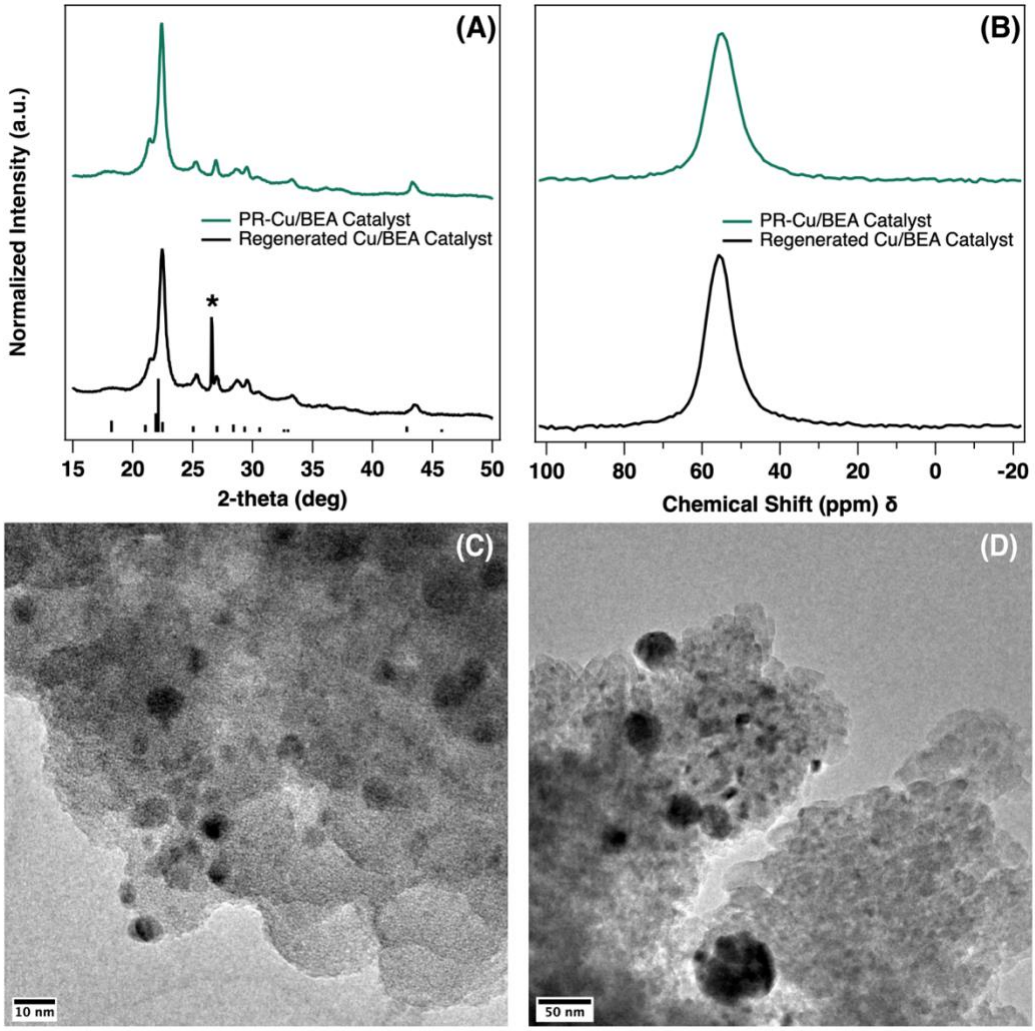

Fig. 7. (A) XRD patterns of PR and regenerated catalysts, where * indicates reflection from residual quartz packing used in the reactor. (B) Solid-state magic angle spinning ^{27}Al NMR spectra of PR and regenerated catalysts. The resonance centered at 50 – 60 ppm is characteristic of tetrahedral Al in the BEA structure (i.e., framework Al). (C) and (D) TEM images of regenerated Cu/BEA catalyst at different magnifications showing both small and large Cu particles consistent with previously published results. [13]

As shown in Fig. 6, catalytic performance of the Cu/BEA catalyst after two forced regeneration cycles resembled that of the fresh catalyst, evidenced by the three stages of the hydrocarbon pool chemistry proceeding similarly before and after the forced regenerations. Compared to the fresh catalyst, the regenerated Cu/BEA catalyst achieved a slightly higher DME conversion and C_{5+} hydrocarbon yield during the induction period (i.e., maximum conversion) and after the reaction reached steady state. This slight improvement in activity may be attributed to more efficient activation of the catalyst in flowing air in the reactor tube compared to calcination in a muffle furnace with limited air flow during preparation of the fresh catalyst. The further minor enhancement in activity with increased regeneration temperature from 450 °C to 500 °C supports this concept of a more efficient activation. Importantly, the hydrocarbon product selectivity did not change after the catalyst regeneration procedures during the induction period (Fig. S8) or at steady state (Fig. 6B). Therefore, the catalytic performance of Cu/BEA was fully recovered, confirming the value of fundamental characterization to inform catalyst regeneration.

4. Conclusions

Inspired by the exceptional catalytic performance of the Cu/BEA catalyst for DME conversion to HOG, we investigated the identity of the carbon species deposited during the reaction and the subsequent carbon removal necessary for regeneration of this catalyst. Applying complementary *ex situ* and *in situ* characterization techniques, we identified that the formation of aromatics, especially polycyclic aromatics, was suppressed on Cu/BEA compared to unmodified BEA, and the graphitic carbon was more hydrogenated and defective. Compared to the extended graphitic surface carbon species observed after high-temperature MTH reactions, DR-UV-vis spectroscopy indicated an abundance of molecular hydrocarbon species and a substantially lower relative amount of graphitic carbon species for the catalysts after the lower temperature DME-to-

HOG reaction. Furthermore, analysis of the carbon removal on post-reaction catalysts using TGA-FTIR spectroscopy and *in situ* DR-UV-vis and Raman spectroscopies demonstrated that the addition of Cu promoted the oxidation of the surface hydrocarbon and graphitic carbon species at lower temperature by activating oxygen. Lastly, guided by the understanding of the carbon species on the catalyst, an effective and efficient regeneration procedure was designed and demonstrated through a series of forced regenerations during the DME-to-HOG reaction over the Cu/BEA catalyst. This regeneration procedure enabled full recovery the catalytic performance. The ability to regenerate this catalyst aids the transition from fundamental catalyst development to applied catalysis, where the ability to utilize the Cu/BEA catalyst with multiple regenerations will be a critical factor in commercial process design and economic models.

Appendix A: Supplementary Material

Supplementary material related to this article can be found, in the online version, at:

Declaration of Competing Interests

The authors declare no competing financial interests.

Acknowledgements

This work was authored by the National Renewable Energy Laboratory, operated by Alliance for Sustainable Energy, LLC, for the U.S. Department of Energy (DOE) under Contract No. DE-AC36-08GO28308. Funding provided by U.S. DOE Office of Energy Efficiency and Renewable Energy Bioenergy Technologies Office. This research was conducted in collaboration with the Chemical Catalysis for Bioenergy (ChemCatBio) Consortium, a member of the Energy Materials Network (EMN). The views expressed in this article do not necessarily represent the views of the DOE or the U.S. Government. The U.S. Government retains and the publisher, by

accepting the article for publication, acknowledges that the U.S. Government retains a nonexclusive, paid-up, irrevocable, worldwide license to publish or reproduce the published form of this work, or allow others to do so, for U.S. Government purposes. The authors thank Dr. Mathew Yung (NREL) for help with XRD measurement and Dr. Jesse Hensley (NREL) for helpful discussion.

Corresponding Authors

*Dan.Ruddy@nrel.gov *Susan.Habas@nrel.gov

Table of Contents Image

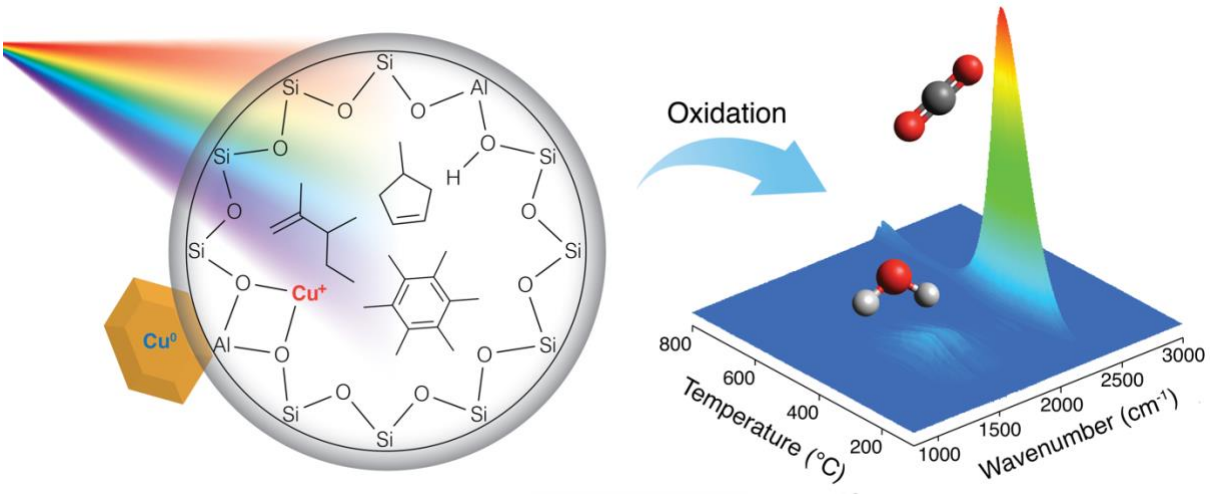

References

1. C.D. Chang, A.J. Silvestri, J. Catal. 47 (1977) 249-259.

2. P. Tian, Y. Wei, M. Ye, Z. Liu, ACS Catal. 5 (2015) 1922-1938.

3. I. Yarulina, A.D. Chowdhury, F. Meirer, B.M. Weckhuysen, J. Gascon, Nat. Catal. 1 (2018) 398-411.

4. I. Yarulina, K. De Wispelaere, S. Bailleul, J. Goetze, M. Radersma, E. Abou-Hamad, I. Vollmer, M. Goesten, B. Mezari, E.J.M. Hensen, J.S. Martínez-Espín, M. Morten, S. Mitchell, J. Perez-Ramirez, U. Olsbye, B.M. Weckhuysen, V. Van Speybroeck, F. Kapteijn, J. Gascon, Nat. Chem. 10 (2018) 804-812.

5. J.H. Ahn, B. Temel, E. Iglesia, Angew. Chem. Int. Ed. 48 (2009) 3814-3816.

6. D.A. Simonetti, J.H. Ahn, E. Iglesia, J. Catal. 277 (2011) 173-195.

7. N. Hazari, E. Iglesia, J.A. Labinger, D.A. Simonetti, Acc. Chem. Res. 45 (2012) 653-662.

8. D.A. Simonetti, R.T. Carr, E. Iglesia, J. Catal. 285 (2012) 19-30.

9. U. Olsbye, S. Svelle, M. Bjørgen, P. Beato, T.V.W. Janssens, F. Joensen, S. Bordiga, K.P. Lillerud, Angew. Chem. Int. Ed. 51 (2012) 5810-5831.

10. U. Olsbye, S. Svelle, K.P. Lillerud, Z.H. Wei, Y.Y. Chen, J.F. Li, J.G. Wang, W.B. Fan, Chem. Soc. Rev. 44 (2015) 7155-7176.

11. L. Qi, Y. Wei, L. Xu, Z. Liu, ACS Catal. 5 (2015) 3973-3982.

12. J. Li, Z. Wei, Y. Chen, B. Jing, Y. He, M. Dong, H. Jiao, X. Li, Z. Qin, J. Wang, W. Fan, J. Catal. 317 (2014) 277-283.

13. J.A. Schaidle, D.A. Ruddy, S.E. Habas, M. Pan, G. Zhang, J.T. Miller, J.E. Hensley, ACS Catal. 5 (2015) 1794-1803.

14. J. Goetze, F. Meirer, I. Yarulina, J. Gascon, F. Kapteijn, J. Ruiz-Martínez, B.M. Weckhuysen, ACS Catal. 7 (2017) 4033-4046.

15. S. Ilias, A. Bhan, ACS Catal. 3 (2013) 18-31.

16. D.A. Simonetti, J.H. Ahn, E. Iglesia, ChemCatChem 3 (2011) 704-718.

17. C.A. Farberow, S. Cheah, S. Kim, J.T. Miller, J.R. Gallagher, J.E. Hensley, J.A. Schaidle, D.A. Ruddy, ACS Catal. 7 (2017) 3662-3667.

18. D.A. Ruddy, J.E. Hensley, C.P. Nash, E.C.D. Tan, E. Christensen, C.A. Farberow, F.G. Baddour, K.M. Van Allsburg, J.A. Schaidle, Nat. Catal. 2 (2019) 632-640.

19. W. Dai, G. Wu, L. Li, N. Guan, M. Hunger, ACS Catal. 3 (2013) 588-596.

20. J.E. Schmidt, J.D. Poplawsky, B. Mazumder, Ö. Attila, D. Fu, D.A.M. de Winter, F. Meirer, S.R. Bare, B.M. Weckhuysen, Angew. Chem. Int. Ed. 55 (2016) 11173-11177.

21. M. Bjørgen, S. Akyalcin, U. Olsbye, S. Benard, S. Kolboe, S. Svelle, J. Catal. 275 (2010) 170-180.

22. J. Goetze, I. Yarulina, J. Gascon, F. Kapteijn, B.M. Weckhuysen, ACS Catal. 8 (2018) 2060-2070.

23. C. Wang, J. Xu, F. Deng, ChemCatChem 12 (2020) 965-980.

24. S. Xu, A. Zheng, Y. Wei, J. Chen, J. Li, Y. Chu, M. Zhang, Q. Wang, Y. Zhou, J. Wang, F. Deng, Angew. Chem. Int. Ed. 52 (2013) 11564-11568.

25. J.F. Haw, J.B. Nicholas, W. Song, F. Deng, Z. Wang, T. Xu, C.S. Heneghan, J. Am. Chem. Soc. 122 (2000) 4763-4775.

26. T. Xu, D.H. Barich, P.W. Goguen, W. Song, Z. Wang, J.B. Nicholas, J.F. Haw, J. Am. Chem. Soc. 120 (1998) 4025-4026.

27. E. Borodina, H. Sharbini Harun Kamaluddin, F. Meirer, M. Mokhtar, A.M. Asiri, S.A. Al-Thabaiti, S.N. Basahel, J. Ruiz-Martinez, B.M. Weckhuysen, ACS Catal. 7 (2017) 5268-5281.

28. S.L. Scott, ACS Catal. 8 (2018) 8597-8599.

29. W. Dai, X. Wang, G. Wu, N. Guan, M. Hunger, L. Li, ACS Catal. 1 (2011) 292-299.

30. M. Bjørgen, F. Bonino, S. Kolboe, K.-P. Lillerud, A. Zecchina, S. Bordiga, J. Am. Chem. Soc. 125 (2003) 15863-15868.

31. E.C. Nordvang, E. Borodina, J. Ruiz-Martínez, R. Fehrmann, B.M. Weckhuysen, Chem. Eur. J. 21 (2015) 17324-17335.

32. L. Palumbo, F. Bonino, P. Beato, M. Bjørgen, A. Zecchina, S. Bordiga, J. Phys. Chem. 112 (2008) 9710-9716.

33. T. Smausz, B. Kondász, T. Gera, T. Ajtai, N. Utry, M. Pintér, G. Kiss-Albert, J. Budai, Z. Bozóki, G. Szabó, B. Hopp, Appl. Phys. 123 (2017) 633.

34. M. Taniguchi, J.S. Lindsey, Photochem. Photobiol. 94 (2018) 290-327.

35. S. Bordiga, C. Lamberti, F. Bonino, A. Travert, F. Thibault-Starzyk, Chem. Soc. Rev. 44 (2015) 7262-7341.

36. A.C. Ferrari, Phys. Rev. 61 (2000) 14095-14107.

37. M.W. Smith, I. Dallmeyer, T.J. Johnson, C.S. Brauer, J.-S. McEwen, J.F. Espinal, M. Garcia-Perez, Carbon 100 (2016) 678-692.

38. E. Borodina, F. Meirer, I. Lezcano-González, M. Mokhtar, A.M. Asiri, S.A. Al-Thabaiti, S.N. Basahel, J. Ruiz-Martinez, B.M. Weckhuysen, ACS Catal. 5 (2015) 992-1003.

39. S. Müller, Y. Liu, M. Vishnuvarthan, X. Sun, A.C. van Veen, G.L. Haller, M. Sanchez-Sanchez, J.A. Lercher, J. Catal. 325 (2015) 48-59.

40. Zachariou, A. Hawkins, D. Lennon, S.F. Parker, Suwardiyanto, S.K. Matam, C.R.A. Catlow, P. Collier, A. Hameed, J. McGregor, R.F. Howe, Appl. Catal. A Gen. 569 (2019) 1-7.

41. Suwardiyanto, R.F. Howe, E.K. Gibson, C.R.A. Catlow, A. Hameed, J. McGregor, P. Collier, S.F. Parker, D. Lennon, Faraday Discuss. 197 (2017) 447-471.

42. E.I. Zabryanskii, V.P. Grebenshchikov, Chem. Tech. 8 (1972) 138-140.

43. E.M. Cordi, P.J. O'Neill, J.L. Falconer, Appl. Catal. B Environ. 14 (1997) 23-36.

44. P.M. Heynderickx, J.W. Thybaut, H. Poelman, D. Poelman, G.B. Marin, J. Catal. 272 (2010) 109-120.

45. V. Balcaen, H. Poelman, D. Poelman, G.B. Marin, J. Catal. 283 (2011) 75-88.

46. N.R. Dhineshbabu, V. Rajendran, N. Nithyavathy, R. Vetumperumal, Appl. Nanosci. 6 (2016) 933-939.

47. F. Giordanino, P.N. Vennestrøm, L.F. Lundegaard, F.N. Stappen, S. Mossin, P. Beato, S. Bordiga, C. Lamberti, Dalton Trans. 42 (2013) 12741-61.

48. M. Argyle, C. Bartholomew, Catalysts 5 (2015) 145-269.

49. J. Zhou, J. Zhang, Y. Zhi, J. Zhao, T. Zhang, M. Ye, Z. Liu, Ind. Eng. Chem. Res. 57 (2018) 17338-17347.